12-12-2021

Effect of Laplace-Domain Theodorsen Function on the Aeroelasticity of Typical Sections

Steve Park
Washington University in St. Louis

Mechanical Engineering and Materials Science

Effect of Laplace-Domain Theodorsen Function on the Aeroelasticity of Typical Sections

Steve Park

steve.park@wustl.edu

Undergraduate Researcher

Washington University in St. Louis

St. Louis, MO, USA

Dr. David Peters

dap@wustl.edu

McDonell Douglas Professor

Washington University in St. Louis

St. Louis, MO, USA

Table of Contents

Abstract

In the analysis of flutter of fixed-wing aircraft, it is common to use the "p-k" method in which one iterates on the reduced frequency of the Theordorsen aerodynamic theory based on the Imaginary part of the eigenvalue. However, this process only is correct when the real part of the eigenvalue is zero (*i.e.*, at the stability boundary) because Theodorsen assumes simple harmonic motion. In this paper, we investigate the accuracy of this method for eigenvalues away from the stability bound by replacing the Theodorsen function C(k) with its aerodynamic counterpart for growing or decaying motion. We then study the accuracy of the p-k method as compared to an exact representation.

Nomenclature

a	slope of the lift curve
b	blade semi-chord, m
e	eigenvalue of matrix E
k	reduced frequency
s	Laplace transform variable in reduced time
$C(k)$	Theodorsen function
$C_M(t)$	coefficients of aerodynamic force corresponding to pitch moment
$C_L(t)$	coefficients of aerodynamic force corresponding to pitch lift
$D(s)$	complex lift deficiency function
I	identity matrix
$Im[e]$	imaginary part of eigenvalue
J_0	Bessel function of the first kind – order zero
J_1	Bessel function of the first kind – order one
$K_0(s)$	Modified Bessel function of the first kind – order zero
$K_1(s)$	Modified Bessel function of the first kind – order one
$Re[e]$	real part of eigenvalue
V	velocity
V^*	normalized velocity
Y_0	Bessel function of the second kind – order zero

Y_1	Bessel function of the second kind – order one
α_{qs}	quasi-steady angle of attack
r_α	radius of gyration
x_α	distance to the center of gravity
ω_α	pitch frequency
$\bar{\omega}_\alpha$	non-dimensional pitch frequency
ω_h	plunge frequency
$\bar{\omega}_h$	non-dimensional plunge frequency
κ	aerodynamic parameter

Introduction

Flutter is the dynamic aeroelasticity phenomenon whereby the inertia forces can modify the behavior of a flexible system so that energy is extracted from the incoming flow [1]. The classical flutter of a typical airfoil section is given in Eq. 1.

$$r_\alpha^2\ddot{\alpha} + \frac{x_\alpha}{b}\ddot{h} + \omega_\alpha^2 r_\alpha^2 = 2\frac{\kappa}{\pi}\left(\frac{V}{b}\right)^2 C_M(t)$$

$$x_\alpha\ddot{\alpha} + \frac{1}{b}\ddot{h} + \frac{\omega_h^2}{b}h = \frac{\kappa}{\pi}\left(\frac{V}{b}\right)^2 C_L(t) \tag{1}$$

$\alpha_{qs}, C_M(t), C_L(t)$ in the classical flutter equation are defined in Eq. 2, 3 and 4.

$$\alpha_{qs} = \frac{\dot{h}}{V} + \alpha + b\left(\frac{1}{2} - a\right)\frac{\dot{\alpha}}{V} \tag{2}$$

$$C_M(t) = -\frac{\pi}{2V^2}\left[\left(\frac{1}{8} + a^2\right)\ddot{\alpha} - ab\ddot{h}\right] + \pi\left(a + \frac{1}{2}\right)C(k)\alpha_{qs} - \frac{\pi}{2V^2}\left[V\left(\frac{1}{2} - a\right)\dot{\alpha}\right] \tag{3}$$

$$C_L(t) = \frac{\pi b}{V^2}\left(V\dot{\alpha} + \ddot{h} - ba\ddot{\alpha}\right) + 2\pi C(k)\alpha_{qs} \tag{4}$$

This analysis assumes that the dynamic lift and pitching moment on the blade are given in terms of Theodorsen Theory and the Theodorsen Function $C(k)$, which is defined in Eq. 5 [3]. J and Y represent the Bessel Function of the first kind and the second kind, respectively.

$$C(k) = \frac{J_1 - iY_1}{J_1 - iY_1 + i(J_0 - iY_0)} \tag{5}$$

However, Theodorsen Theory assumes that the motion of the airfoil is simple harmonic, while the eigenvalue problem for the dynamics of the typical section is not necessarily simple harmonic, but it is written in terms of the Laplace variable s which has both real and imaginary parts. Thus, the solution of this classical problem is only valid for a root that is exactly at the stability boundary so that the Re(s) = 0. A complex version of the Theodorsen Function exists, which is shown in Eq. 2 [3]. $K(s)$ represents the Modified Bessel Function of the second kind.

$$D(s) = \frac{K_1(s)}{K_0(s) + K_1(s)} \tag{6}$$

Therefore, it is possible to do a complete Laplace Transform solution for the typical section that is not limited to validity only at the stability boundary.

Methodology

After combining equations from Ref. [4] and [5], we came up with three matrices, which are shown in Eq. 7.

$$M = \begin{bmatrix} r_\alpha^2 + \kappa\left(\frac{1}{8} + a^2\right) & x_a - \kappa a \\ x_a - \kappa a & 1 + \kappa \end{bmatrix}$$

$$K = \begin{bmatrix} -2\kappa\left(\frac{1}{2} + a\right)C(k) + \bar{\omega}_\alpha^2 r_\alpha^2 & 0 \\ 2\kappa C(k) & \bar{\omega}_h^2 \end{bmatrix}$$

$$C = \begin{bmatrix} \left(\frac{1}{2} - a\right)\kappa - 2\kappa\left(\frac{1}{4} - a^2\right)C(k) & -2\kappa\left(\frac{1}{2} + a\right)C(k) \\ 2\kappa\left(\frac{1}{2} - a\right)C(k) + \kappa & 2\kappa C(k) \end{bmatrix} \tag{7}$$

Using three matrices from above, we created a new 4×4 matrix E, which is shown in Eq. 8.

$$E = \begin{bmatrix} I & 0 \\ 0 & M^{-1} \end{bmatrix} \begin{bmatrix} 0 & I \\ -K & -C \end{bmatrix} \tag{8}$$

We use $V^*$and $\bar{\omega}_\alpha$ to nondimensionalize the variables and simplify the calculation. $V^*$and $\bar{\omega}_\alpha$ are defined in Eq. 9 and 10, respectively.

$$V^* = \frac{V}{b\omega_\alpha} = \frac{1}{\bar{\omega}_\alpha} \tag{9}$$

$$\bar{\omega}_\alpha = \frac{1}{V^*} \tag{10}$$

We used three $\frac{\bar{\omega}_h}{\bar{\omega}_\alpha}$ ratios for the iterations, and x$\frac{\bar{\omega}_h}{\bar{\omega}_\alpha}$ is defined in Eq. 11.

$$\frac{\bar{\omega}_h}{\bar{\omega}_\alpha} = \frac{\omega_h}{\omega_\alpha} \tag{11}$$

Part A. $C(k)$ iteration

1. Use four different x_α : $0, 0.05, 0.1, 0.2$
2. For each x_α value, use three different $\frac{\bar{\omega}_h}{\bar{\omega}_\alpha}$: 0.1, 0.5, 0.8
3. Find the approximate $\bar{\omega}_\alpha$ value. The best way to find this is approximating the V^* value from Ref. [1] Fig. 3, and calculate $\bar{\omega}_\alpha$ using Eq. 10.
4. Let approximate $\bar{\omega}_\alpha$ value $= (\bar{\omega}_\alpha)_{approx}$
5. Create an array with 20 possible $\bar{\omega}_\alpha$ values. This array ranges from $(\bar{\omega}_\alpha)_{approx} - 0.001$ to $(\bar{\omega}_\alpha)_{approx} + 0.0009$. The array has an interval of 0.0001.
6. Start with $k = 0.15$ (or any k value, preferably k<1) and find four eigenvalues of matrix E.
7. Choose two pairs with $Im[e] > 0$
8. Pick eigenvalue with the real part closer to zero (in other words, smaller absolute value of the real part).
9. Replace the old k with $Im[e]$. Iterate again until k is equal to $Im[e]$, or until k value is constant.
10. Store real part of this eigenvalue for each $\bar{\omega}_\alpha$ value of the array

11. Plot $\bar{\omega}_\alpha$ against $Real[e]$, which is shown in the Results section.

Part B. $D(s)$ iteration

Steps 1 to 5 are the same as $C(k)$ iteration.

6. Start with any s value with both real and imaginary parts. Any s value will yield the same result. We started the iteration with $s = 0.0003 + 0.16i$. Find four eigenvalues of matrix E.
7. Choose two pairs with $Im[e] > 0$.
8. Pick eigenvalue with the real part closer to zero (in other words, smaller absolute value of the real part).
9. Replace the old s value with the chosen eigenvalue. Iterate again until s is equal to eigenvalue, or until s is constant.
10. Store real part of this eigenvalue for each $\bar{\omega}_\alpha$ value of the array.
11. Plot $\bar{\omega}_\alpha$ against $Real[e]$, which is shown in the Results section.

Results

Part A. Variations in vicinity of the boundary. $x_\alpha = 0, \frac{\bar{\omega}_h}{\bar{\omega}_\alpha} = 0.1, 0.5, 0.8$

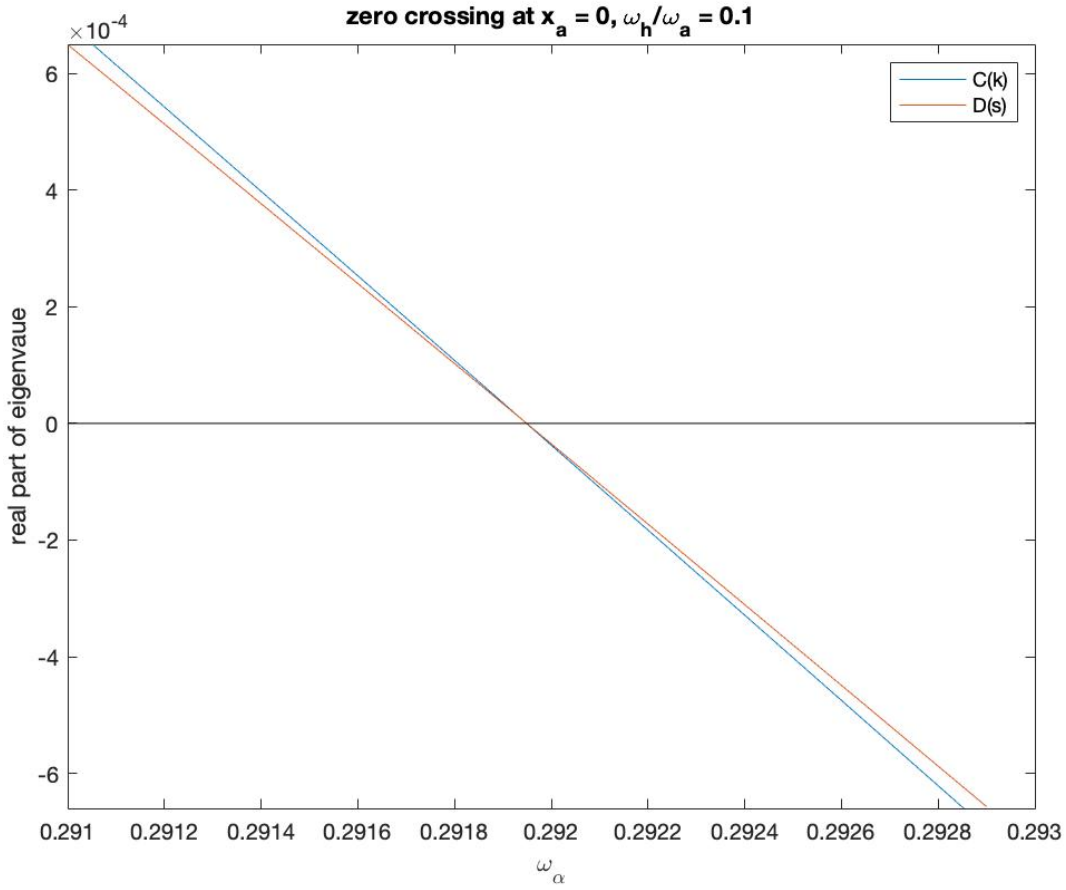

Figure 1. $C(k)$ and $D(s)$ Iteration at $x_\alpha = 0$, $\frac{\bar{\omega}_h}{\bar{\omega}_\alpha} = 0.1$

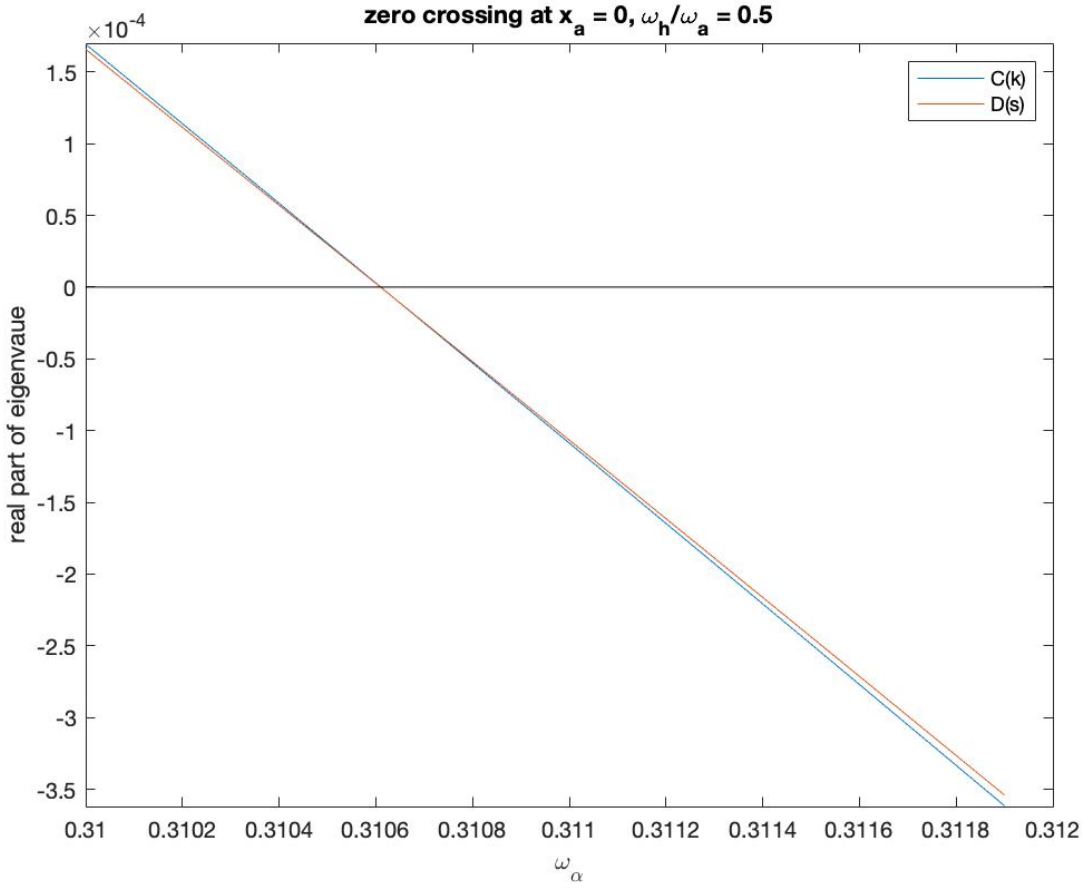

Figure 2. $C(k)$ and $D(s)$ Iteration at $x_\alpha = 0,\ \frac{\bar{\omega}_h}{\bar{\omega}_\alpha} = 0.5$

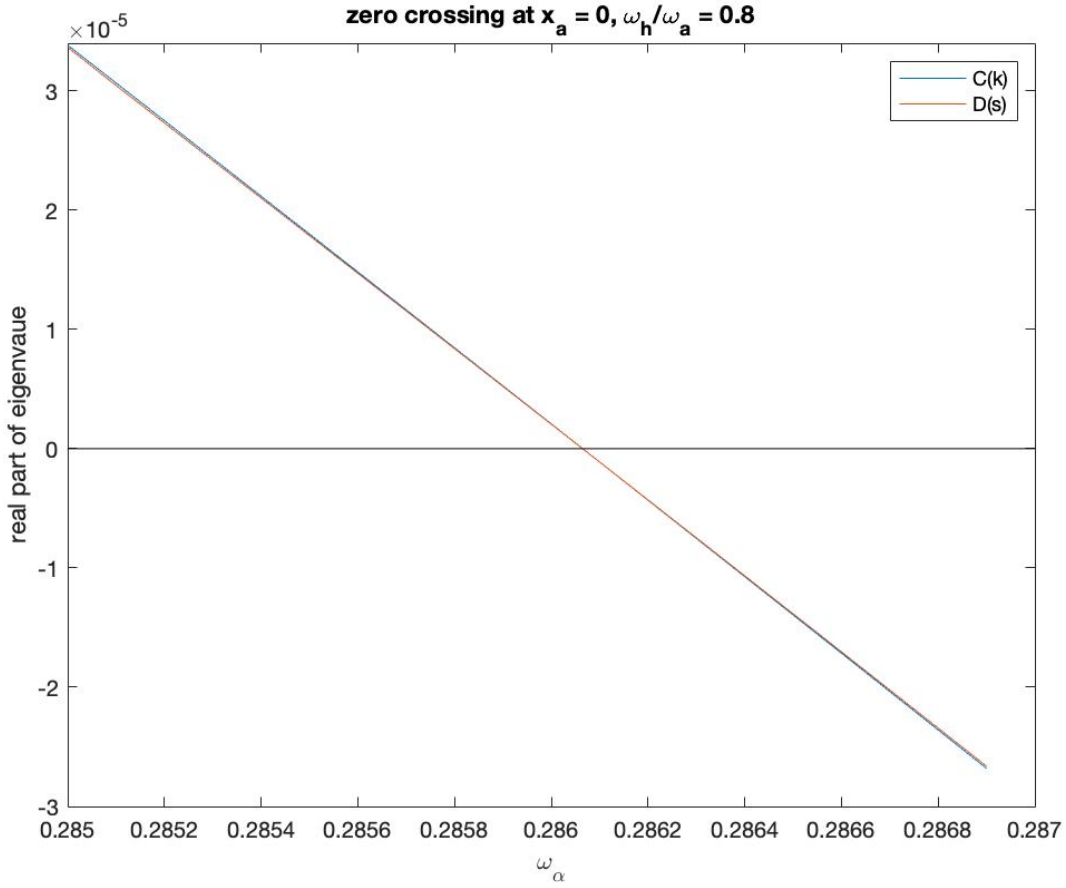

Figure 3. $C(k)$ and $D(s)$ Iteration at $x_\alpha = 0$, $\frac{\bar{\omega}_h}{\bar{\omega}_\alpha} = 0.8$

The main focus of this iteration is to observe if the $C(k)$ and $D(s)$ iterations cross each other at the real part of eigen value equal to zero. As shown in Fig. 3, 4, and 5, $C(k)$ and $D(s)$ iterations for various $\frac{\bar{\omega}_h}{\bar{\omega}_\alpha}$ all cross each other at $real(e) = 0$. We can also observe that as $\frac{\bar{\omega}_h}{\bar{\omega}_\alpha}$ increases, the gap between C(k) and $D(s)$ becomes narrower. The graph depicts both C(k) and $D(s)$ iterations as linear plots, but they look linear because the plot has such a narrow ω_α range. The same plot with a wider ω_α range is shown in Part E. The main conclusion is that the effect of replacing C(k) with D(s) for small variations from the stability boundary is a linear effect with frequency rather than quadratic.

Part B. Small variations with aero offset. $\boldsymbol{x_\alpha = 0.05, \frac{\bar{\omega}_h}{\bar{\omega}_\alpha} = 0.1, 0.5, 0.8}$

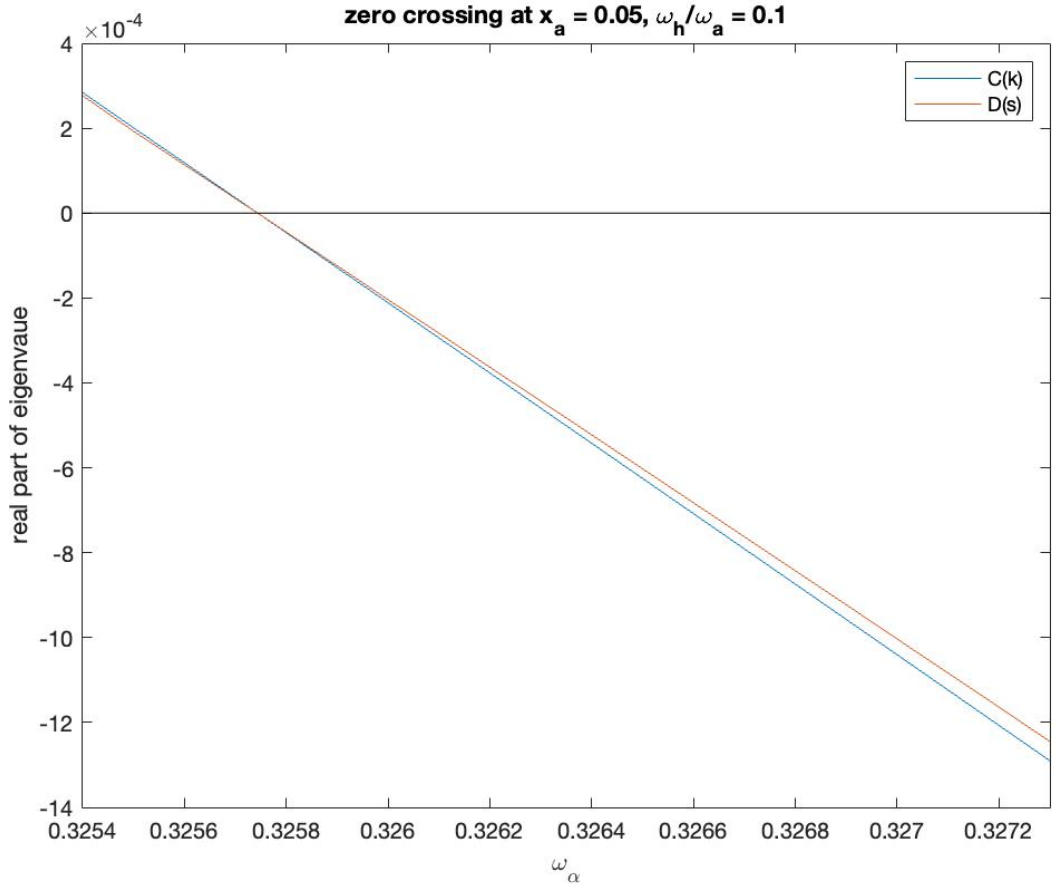

Figure 4. $C(k)$ and $D(s)$ Iteration at $x_\alpha = 0.05,\ \frac{\bar{\omega}_h}{\bar{\omega}_\alpha} = 0.1$

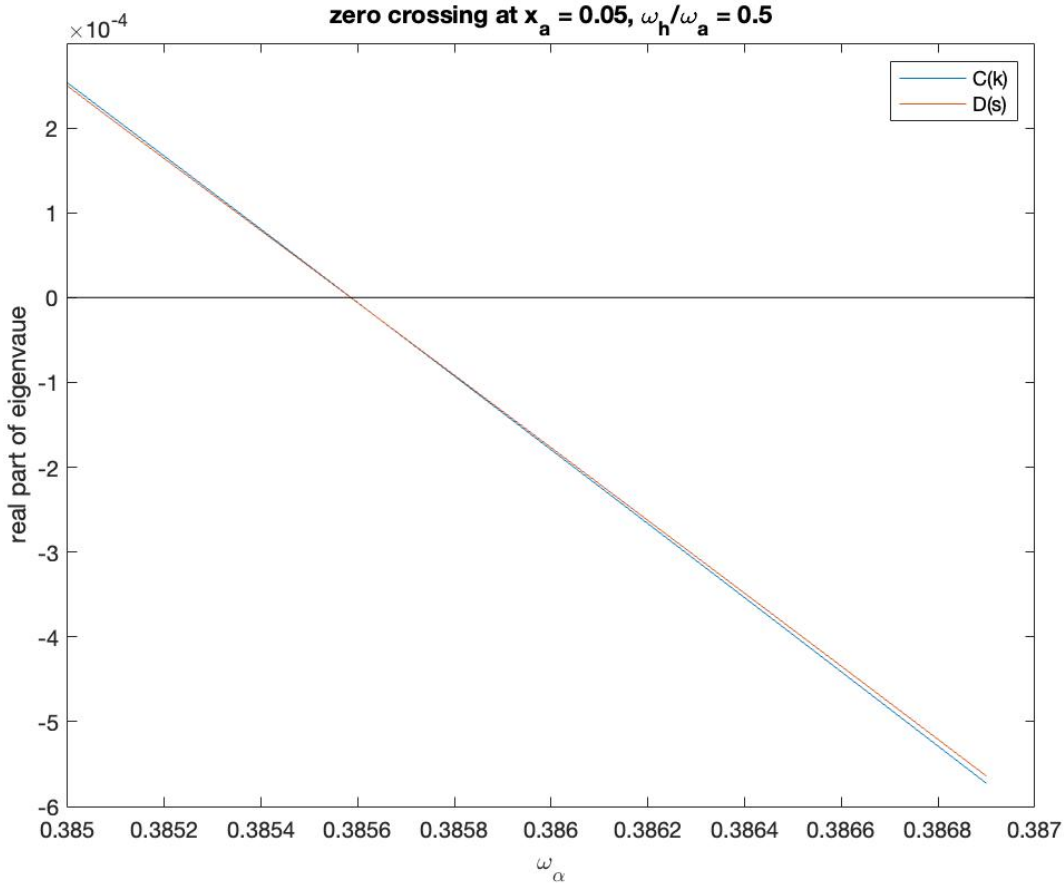

Figure 5. $C(k)$ and $D(s)$ Iteration at $x_\alpha = 0.05,\ \frac{\bar{\omega}_h}{\bar{\omega}_\alpha} = 0.5$

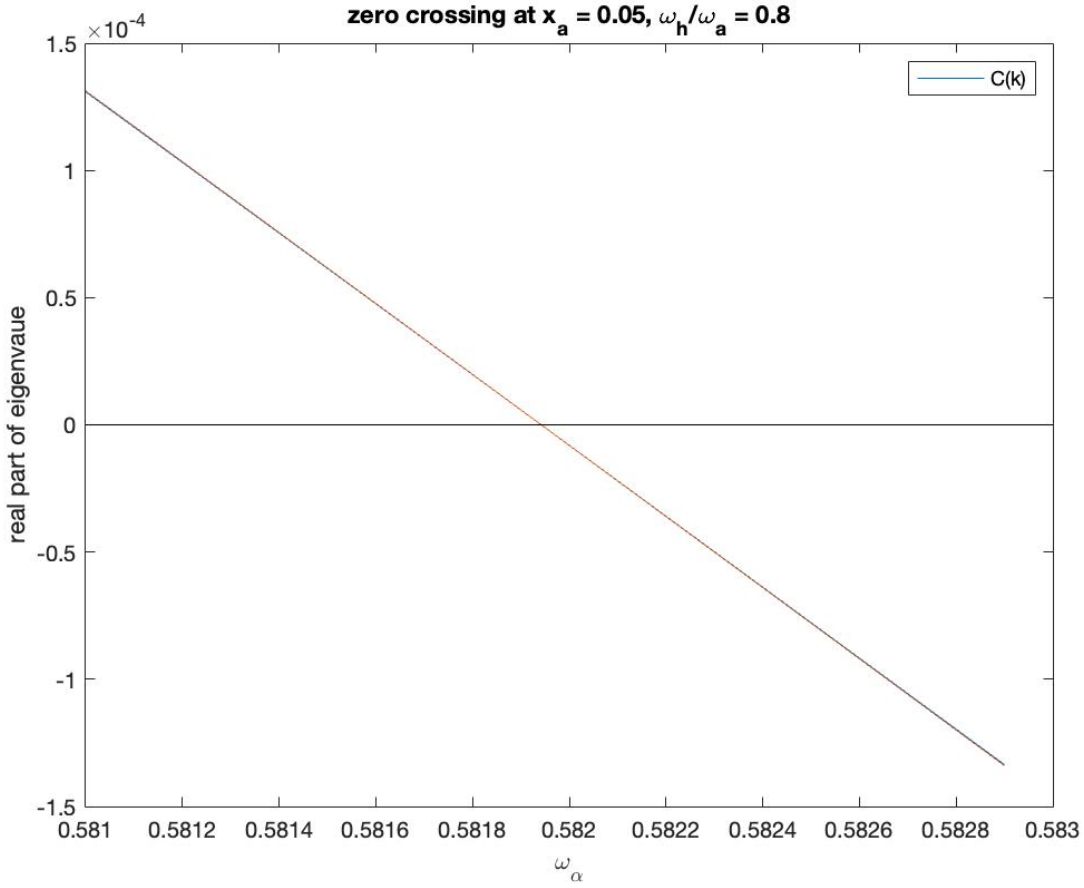

Figure 6. $C(k)$ and $D(s)$ Iteration at $x_\alpha = 0.05,\ \frac{\bar{\omega}_h}{\bar{\omega}_\alpha} = 0.8$

These show the same trends as without aerodynamic offset.

Part C. Still larger aero offset. $\boldsymbol{x_\alpha = 0.1, \frac{\bar{\omega}_h}{\bar{\omega}_\alpha} = 0.1, 0.5, 0.8}$

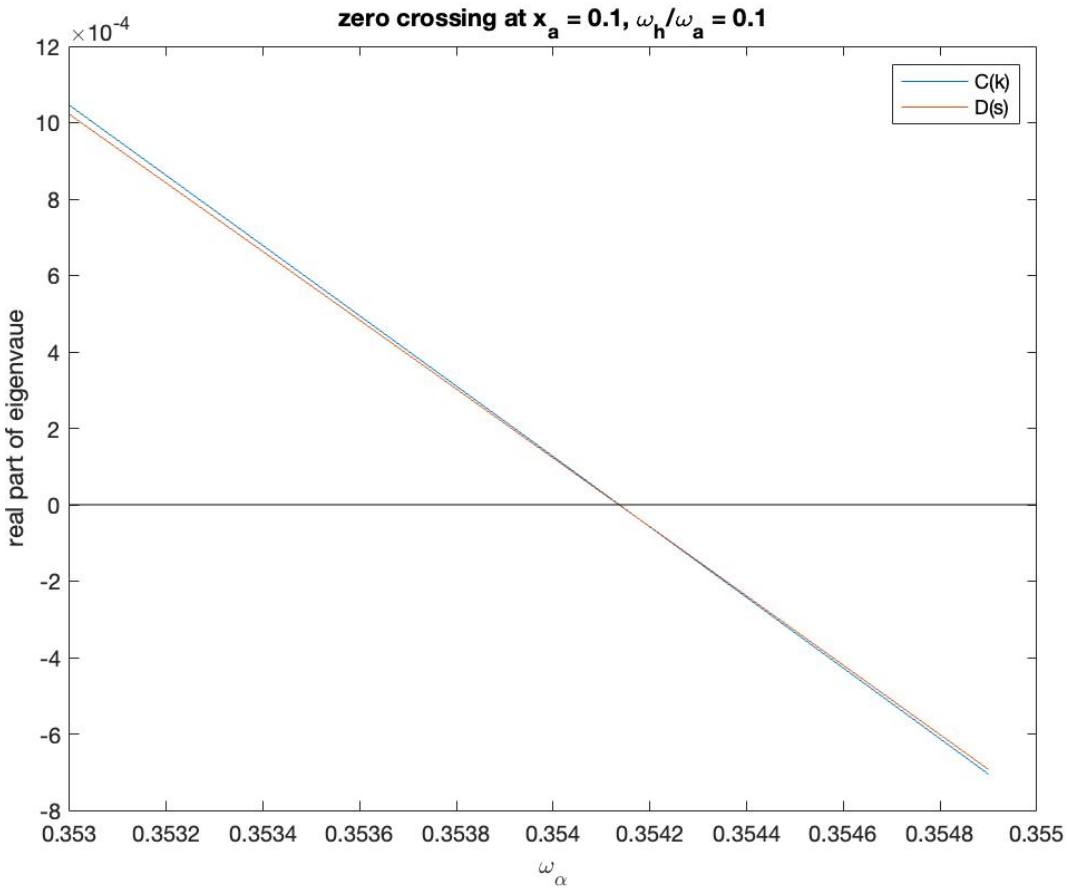

Figure 7. $C(k)$ and $D(s)$ Iteration at $x_\alpha = 0.1,\ \frac{\bar{\omega}_h}{\bar{\omega}_\alpha} = 0.1$

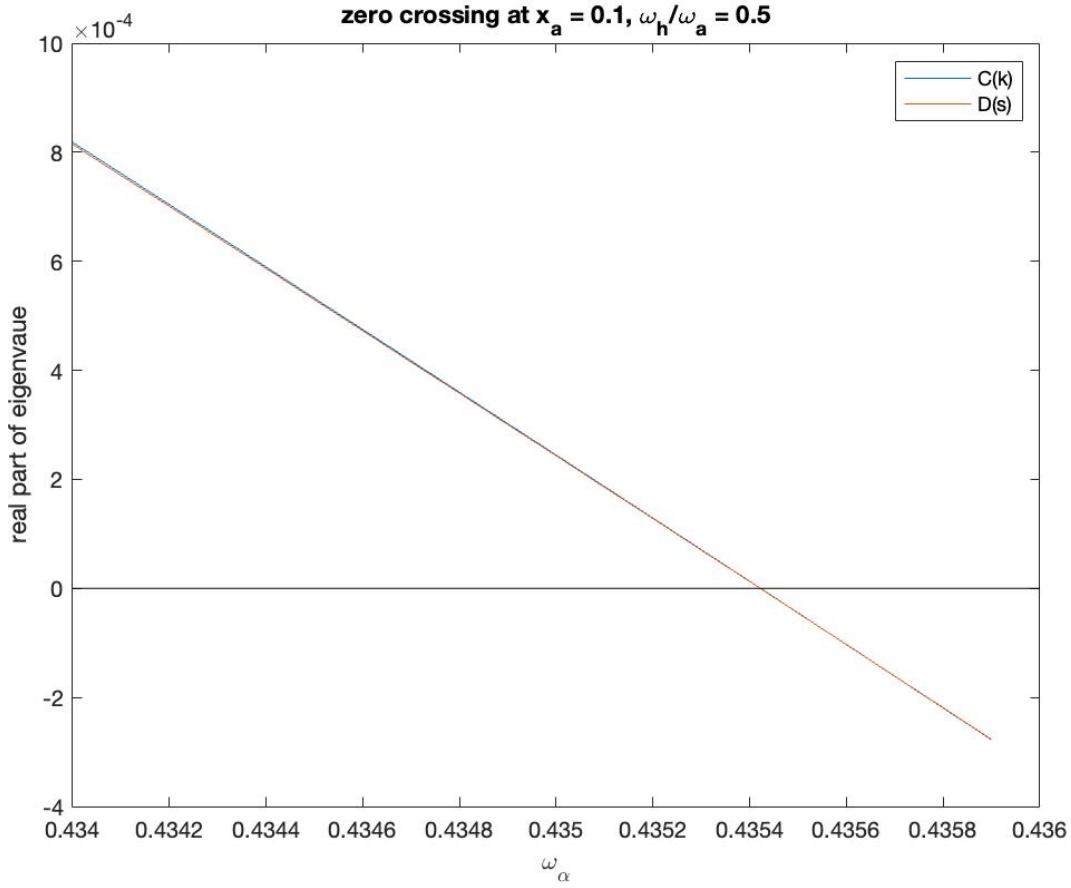

Figure 8. $C(k)$ and $D(s)$ Iteration at $x_\alpha = 0.1$, $\frac{\bar{\omega}_h}{\bar{\omega}_\alpha} = 0.5$

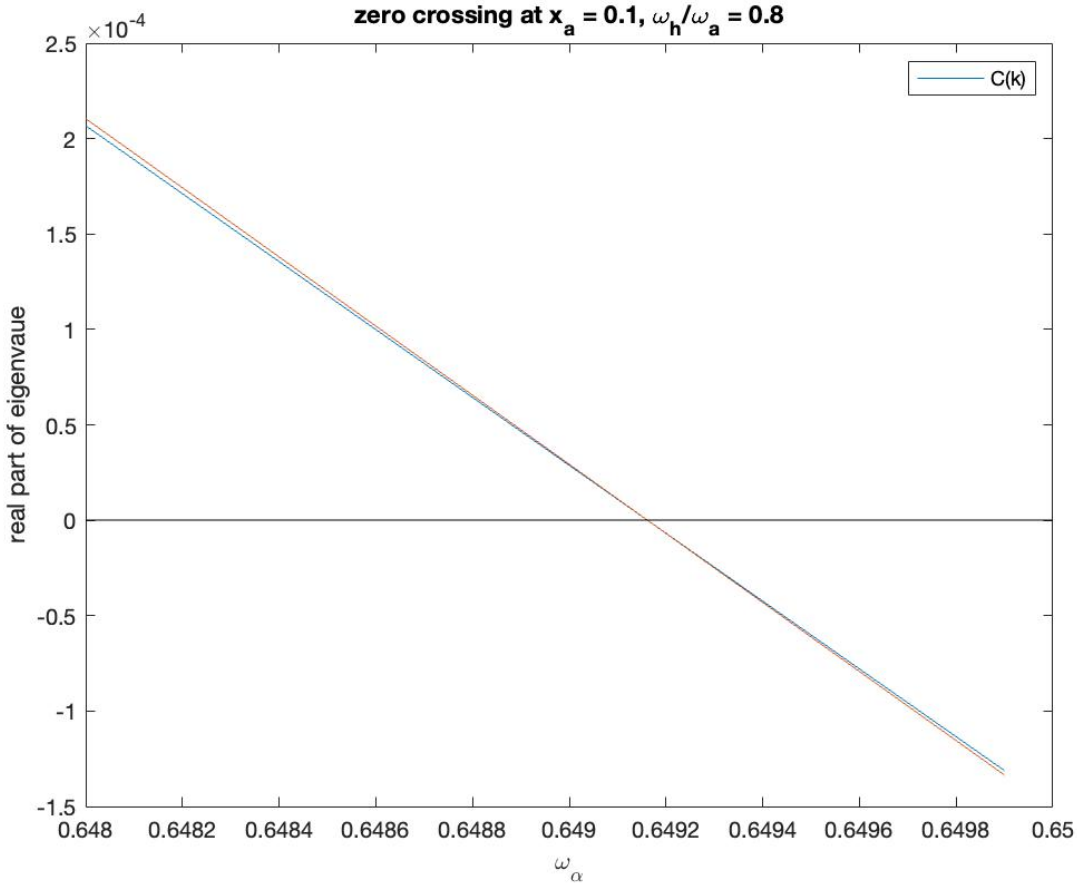

Figure 9. $C(k)$ and $D(s)$ Iteration at $x_\alpha = 0.1,\ \frac{\bar{\omega}_h}{\bar{\omega}_\alpha} = 0.8$

We thus see that the larger the offset, the less is the effect of D(s) on the eigenvalue in the vicinity of the stability boundary.

Part D. Effect of ratio of bending frequency to torsion frequency.

$$x_\alpha = 0.05, \frac{\bar{\omega}_h}{\bar{\omega}_\alpha} = 0.1, 0.5, 0.8$$

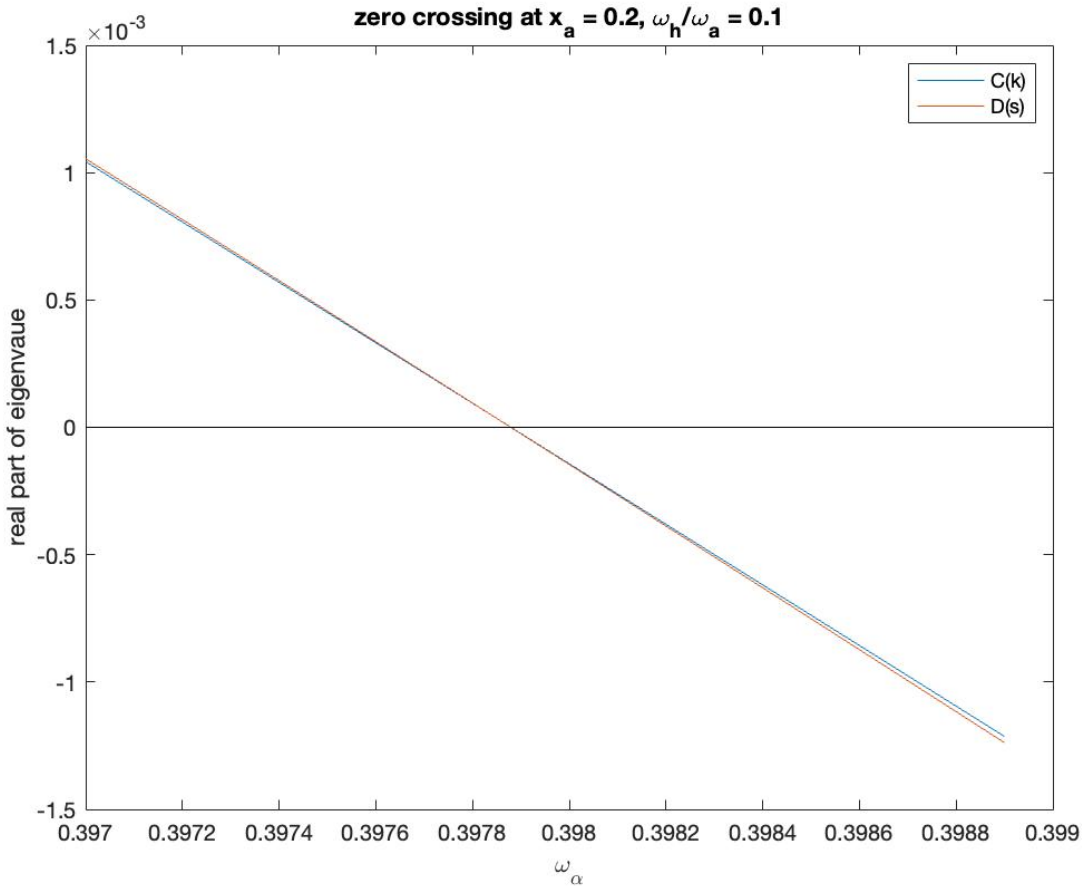

Figure 10. $C(k)$ and $D(s)$ Iteration at $x_\alpha = 0.2$, $\frac{\bar{\omega}_h}{\bar{\omega}_\alpha} = 0.1$

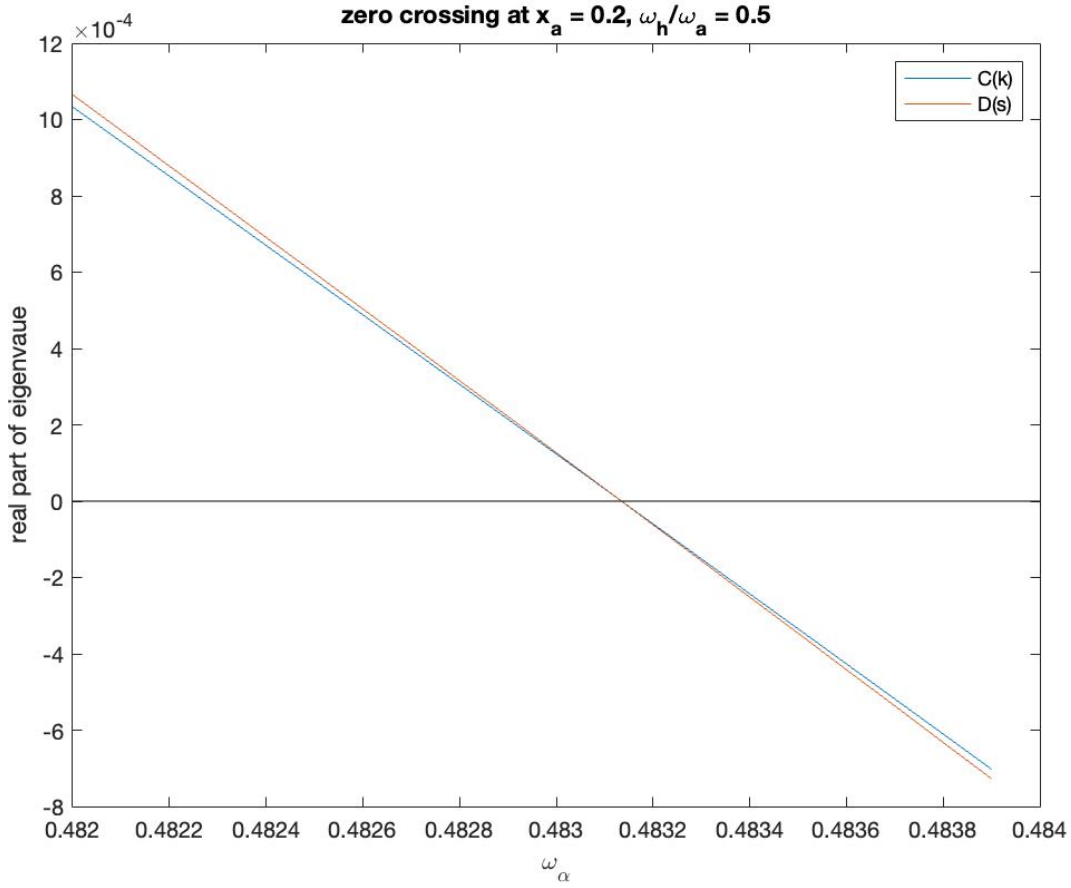

Figure 11. $C(k)$ and $D(s)$ Iteration at $x_\alpha = 0.2,\ \frac{\bar{\omega}_h}{\bar{\omega}_\alpha} = 0.5$

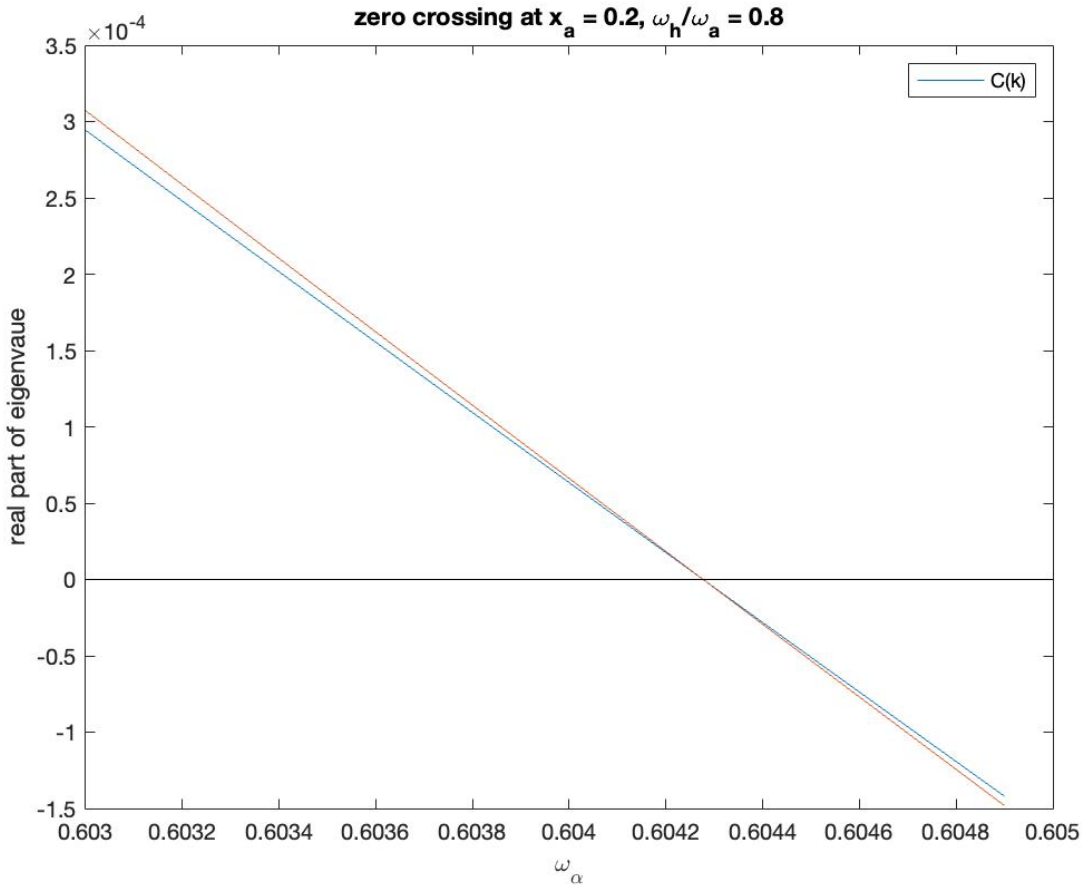

Figure 12. $C(k)$ and $D(s)$ Iteration at $x_\alpha = 0.2,\ \frac{\bar{\omega}_h}{\bar{\omega}_\alpha} = 0.8$

Thus, the same results hold at other ratios of the bending frequency to the torsion frequency for the Real part of the eigenvalues.

Part E. Larger variations away from stability boundary.

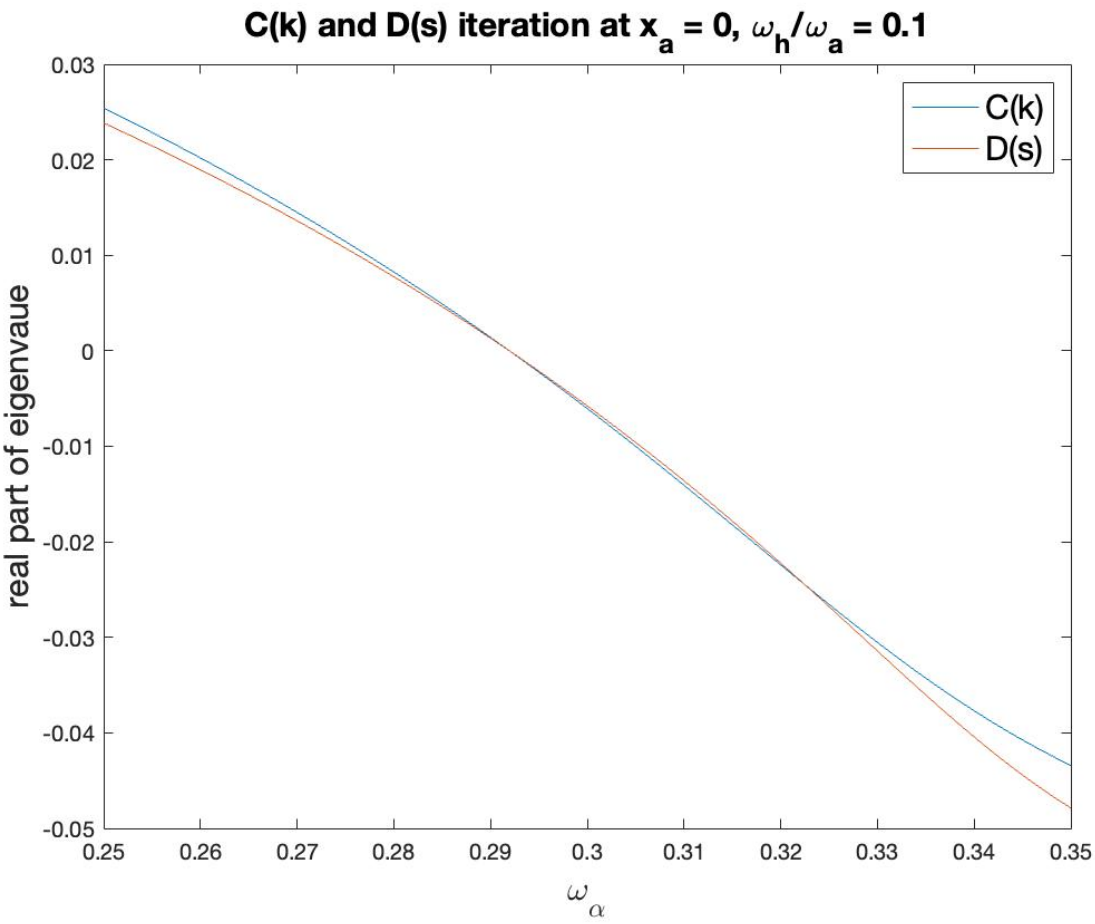

Figure 13. $C(k)$ and $D(s)$ Iteration at $x_\alpha = 0$, $\frac{\bar{\omega}_h}{\bar{\omega}_\alpha} = 0.1$ with wider ω_α range

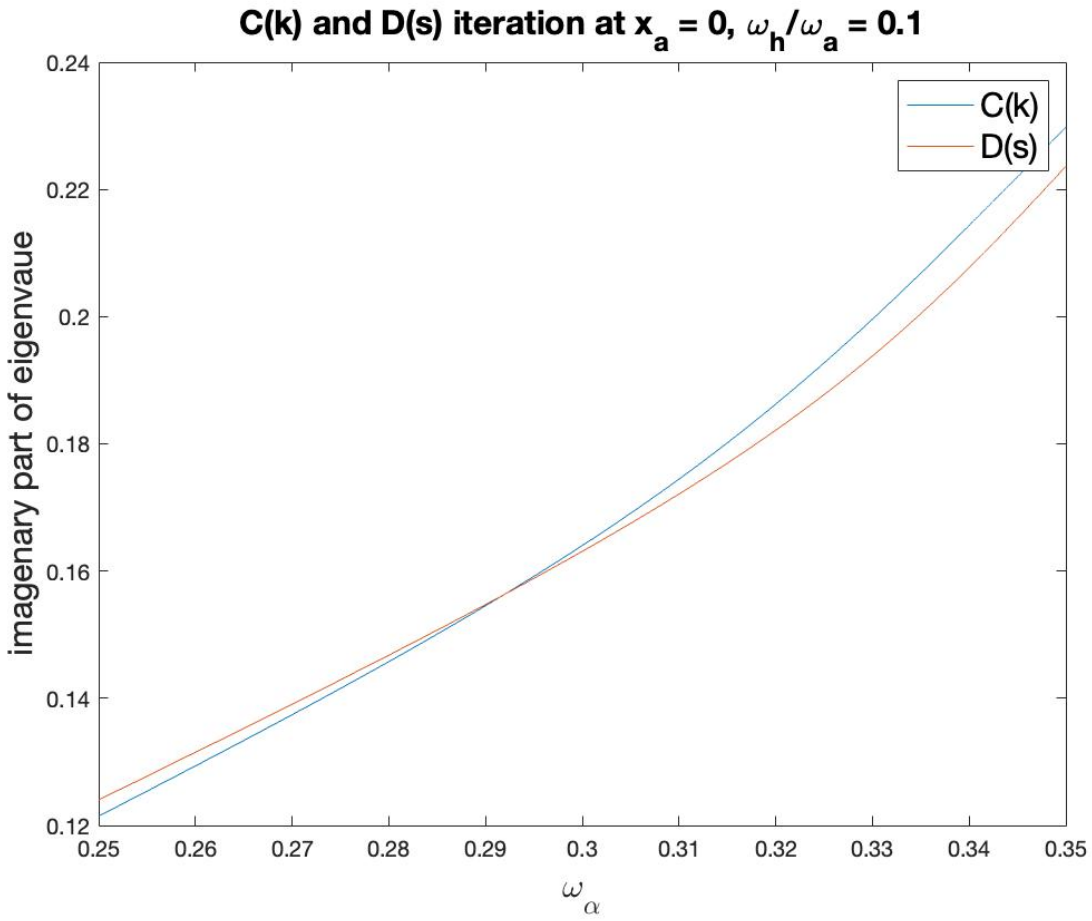

Figure 14. $C(k)$ and $D(s)$ Iteration at $x_\alpha = 0$, $\frac{\bar{\omega}_h}{\bar{\omega}_\alpha} = 0.1$ with imaginary part and wider ω_α range

With the larger variations in frequency, we can see the quadratic effects of D(s) as we move further away from the boundary. This is true both for the damping (the real part) and for the frequency (the imaginary part).

Conclusion

1. The effect of a complex version of aerodynamics being used is seen even for perturbations in parameters as a small but noticeable linear effect.

2. The effect increases with the distance from the stability boundary but remains small.

3. Thus, the presently-used p-k method is fairly accurate.

4. However, there is only a minimal extra effort involved in including the true D(s) so that there is no compelling reason not to include it with its greater accuracy at no additional computational cost.

References

[1] *A Modern Course in Aeroelasticity,* Earl H. Dowell (Editor), Third Edition, Kluwar Academic Publishers, Boston, 1995, Fifth Edition, 2015, pp. 370-437.

[2] Kurniawan, Riccy. "Numerical Study of Flutter of a Two-Dimensional Aeroelastic System." *ISRN Mechanical Engineering*, Hindawi, 8 Dec. 2013.

[3] Peters, David A., "Two-Dimensional Incompressible Unsteady Airfoil Theory – An Overview," Journal of Fluids and Structures, Vol. 24, No. 3, July 2008, pp. 295-312.

[4] Scanlan, Robert H., and Rosenbaum, Robert, *Aircraft Vibration and Flutter,* The MacMillan Company, New York, 1951, pp. 197-201.

[5] Johnson, Wayne, *Helicopter Theory,* Dover Publications, New York, 1980, pp. 479-480.